Perfusion Measurement in Brain Gliomas with Intravoxel Incoherent Motion MRI

C. Federau, R. Meuli, K. O'Brien, P. Maeder, and P. Hagmann

ABSTRACT

BACKGROUND AND PURPOSE: Intravoxel incoherent motion MRI has been proposed as an alternative method to measure brain perfusion. Our aim was to evaluate the utility of intravoxel incoherent motion perfusion parameters (the perfusion fraction, the pseudodiffusion coefficient, and the flow-related parameter) to differentiate high- and low-grade brain gliomas.

MATERIALS AND METHODS: The intravoxel incoherent motion perfusion parameters were assessed in 21 brain gliomas (16 high-grade, 5 low-grade). Images were acquired by using a Stejskal-Tanner diffusion pulse sequence, with 16 values of b (0–900 s/mm^2) in 3 orthogonal directions on 3T systems equipped with 32 multichannel receiver head coils. The intravoxel incoherent motion perfusion parameters were derived by fitting the intravoxel incoherent motion biexponential model. Regions of interest were drawn in regions of maximum intravoxel incoherent motion perfusion fraction and contralateral control regions. Statistical significance was assessed by using the Student t test. In addition, regions of interest were drawn around all whole tumors and were evaluated with the help of histograms.

RESULTS: In the regions of maximum perfusion fraction, perfusion fraction was significantly higher in the high-grade group (0.127 $\pm$ 0.031) than in the low-grade group (0.084 $\pm$ 0.016, $P < .001$) and in the contralateral control region (0.061 $\pm$ 0.011, $P < .001$). No statistically significant difference was observed for the pseudodiffusion coefficient. The perfusion fraction correlated moderately with dynamic susceptibility contrast relative CBV ($r = 0.59$). The histograms of the perfusion fraction showed a "heavy-tailed" distribution for high-grade but not low-grade gliomas.

CONCLUSIONS: The intravoxel incoherent motion perfusion fraction is helpful for differentiating high- from low-grade brain gliomas.

ABBREVIATIONS: D = diffusion coefficient; D^* = pseudodiffusion coefficient; f = perfusion fraction; fD^* = flow-related parameter; IVIM = intravoxel incoherent motion

An estimated 69,720 new cases of primary central nervous system tumors are expected to be diagnosed in the United States in 2013, of which an estimated 24,620 new cases will be malignant (13,630 in males and 10,990 in females).[1] The 5-year relative survival rate following diagnosis of primary malignant CNS tumors, mostly gliomas, is poor, with an average of 33.8%, but it is age-dependent, decreasing monotonically from 73% for 0–19 years of age to 10% for 65–74 years of age (data from 1995–2009).[2]

The assessment of perfusion characteristics of those lesions by using dynamic susceptibility MR imaging has become an important part of the initial evaluation and follow-up because cerebral blood volume has been shown to correlate with the degree of neovascularization[3] and increased local perfusion has been shown to correlate with tumor grading[4] and prognosis.[5] Histologically, the assessment of microvascularity is important for the grading of a primary brain tumor[6] because high-grade neoplasms produce a pathologic microvascular network through neoangiogenesis to satisfy a growing need for nutriments and oxygen.

Le Bihan et al[7] have proposed measuring microvascular perfusion with an MR imaging–based method called intravoxel incoherent motion (IVIM) imaging. The incoherent motion of spins, which can be understood as the spatial "mixing" of spins

Received March 30, 2013; accepted after revision June 2.

From the Department of Diagnostic and Interventional Radiology (C.F., R.M., P.M., P.H.), Centre Hospitalier Universitaire Vaudois and University of Lausanne, Lausanne, Switzerland; and Center for Biomedical Imaging (K.O.), University of Geneva, Geneva, Switzerland.

P. Maeder and P. Hagmann contributed equally to this work.

This work was supported by the Centre d'Imagerie BioMédicale of the University of Lausanne, University of Geneva, Hôpitaux Universitaires de Genève, Centre Hospitalier Universitaire Vaudois, École polytechnique fédérale de Lausanne and the Leenaards and Jeantet Foundations. C. Federau was supported by the Faculté de biologie et de médecine of the University of Lausanne. P Hagmann was supported by a grant from Leenaards Foundation.

Please address correspondence to Christian Federau, MD, Department of Diagnostic and Interventional Radiology, Centre Hospitalier Universitaire Vaudois, Rue du Bugnon 46, 1011 Lausanne, Switzerland: e-mail: christian.federau@chuv.ch

http://dx.doi.org/10.3174/ajnr.A3686

Table 1: Patient demographics, tumor localization, and histologic diagnosis

Grade	Age (yr)	Sex	Localization	Sample Obtained	Pathologic Diagnosis	WHO Grade
High						
1	77	Male	Left parietal lobe	Surgical resection	Glioblastoma multiforme	IV
2	67	Male	Right parietal lobe	Surgical resection	Glioblastoma multiforme	IV
3	84	Female	Left parietal lobe	Stereotaxic biopsy	Glioblastoma multiforme	IV
4	61	Female	Right frontal lobe	Surgical resection	Glioblastoma multiforme	IV
5	60	Male	Right frontal lobe	Surgical resection	Glioblastoma multiforme	IV
6	68	Male	Right insula	Surgical resection	Glioblastoma multiforme	IV
7	73	Male	Right frontotemporal lobes	Surgical resection	Anaplastic oligoastrocytoma	III
8	36	Male	Left insula	Stereotaxic biopsy	Diffuse glioma	III
9	50	Male	Left temporal lobe	Stereotaxic biopsy	Glioblastoma multiforme	IV
10	43	Male	Left temporal lobe	Surgical resection	Glioblastoma multiforme	IV
11	73	Male	Left temporal lobe	Surgical resection	Glioblastoma multiforme	IV
12	53	Male	Left parietal lobe	Surgical resection	Glioblastoma multiforme	IV
13	60	Female	Left operculum	Stereotaxic biopsy	Glioblastoma multiforme	IV
14	24	Male	Left cingulum	Stereotaxic biopsy	Anaplastic oligoastrocytoma	III
15	61	Male	Left temporal lobe	Surgical resection	Glioblastoma multiforme	IV
16	63	Female	Right frontal lobe	Surgical resection	Glioblastoma multiforme	IV
Low						
1	38	Male	Right frontal lobe	Surgical resection	Oligoastrocytoma	II
2	58	Male	Right frontal lobe	Surgical resection	Neuroglial tumor	II
3	54	Male	Left temporo-occipital lobes	Stereotaxic biopsy	Diffuse astrocytoma	II
4	38	Male	Left frontal lobe	Stereotaxic biopsy	Oligodendroglioma	II
5	2	Male	Centered on 3rd ventricle	Stereotaxic biopsy	Pilomyxoid astrocytoma	II

Note:—WHO indicates World Health Organization.

during the time of measurement, reduces exponentially the signal amplitude obtained from a diffusion-weighted sequence such as the Stejskal-Tanner sequence.[8] This incoherent motion arises inevitably from the thermal diffusion characterized by diffusion coefficient (D) and, in biologic perfused tissue, from movements of blood in the microvasculature, called by analogy pseudodiffusion and characterized by pseudodiffusion coefficient (D^*).

Therefore, an IVIM biexponential signal equation[7] has been proposed to model incoherent motion in biologic tissue, with the perfusion fraction (f) describing the fraction of incoherent signal arising from the vascular compartment in each voxel over the total incoherent signal. Furthermore, under the assumption of an isotropic, randomly laid microvascular network, a linear relationship were derived[9] between D^* and fD^* (the scalar multiplication of f and D^*, referred to as the flow-related parameter) and CBV, MTT^{-1}, and CBF, respectively.

Recently, IVIM showed promising results in helping discriminate high- and low-grade tumors, for example in the salivary gland, among Warthin tumors, pleomorphic adenomas, and malignant tumors[10]; in the pancreas between healthy pancreas and pancreatic cancer[11]; or between renal[12] and breast tumor subtypes.[13] In the brain, where initial reports were made,[7,14-19] IVIM perfusion parameters showed recently a gradual increase in response to gradual increase of hypercapnia.[20]

The purpose of this study was to evaluate the utility of IVIM perfusion parameters (f, D^*, and fD^*) to differentiate high- and low-grade brain gliomas.

MATERIALS AND METHODS

Patient Demographics

The present study was approved by the local ethics committee at University of Lausanne. Patient consents were waived. From May 2011 to December 2012, our clinical glioma protocol included an IVIM sequence, which replaced the standard diffusion-weighted sequence. This provided apparent diffusion maps, which are part of the standard glioma evaluation, as well as perfusion-weighted maps, which allowed our exploratory work. Our clinical glioma protocol also included T1-weighted, T2-weighted, DSC perfusion, and T1-weighted postgadolinium sequences. Twenty-one consecutive patients (17 males, 4 females; mean age, 52.3 ± 21.3 years; age range, 2–84 years; Table 1) who had preoperative MR imaging examination, had no relevant treatment history at the time of imaging (such as radio-, chemo-, or antiangiogenic therapy), and had consecutive histopathologic diagnoses were included in the study. The tumor grading was based on World Health Organization criteria and yielded 16 high-grade and 5 low-grade gliomas. Because of the low number of low-grade gliomas found, a complementary study was performed and included 6 further low-grade gliomas diagnosed on radiologic criteria only (On-line Appendix).

Conventional MR Imaging

Conventional MR imaging, DSC, and IVIM were performed during the same procedure to allow direct comparison. The imaging was performed on 3T MR imaging scanners (Trio, Verio, or Skyra; Siemens, Erlangen, Germany) equipped with 32 multichannel receiver head coils. Before the examination, an 18- to 20-ga needle was inserted in either the right or the left antecubital vein. Afterward, T1-weighted sagittal and T2-weighted axial images were acquired.

IVIM MR Imaging

A Stejskal-Tanner diffusion-weighted spin-echo EPI pulse sequence[15] was used, with multiple b-values (0, 10, 20, 40, 80, 110, 140, 170, 200, 300, 400, 500, 600, 700, 800, 900 s/mm^2) in 3 orthogonal directions, and the corresponding trace was calculated. A single acquisition was obtained (no average). The images were orientated axially with a section thickness of 4 mm, an FOV of 297 × 297 mm^2, and a matrix size of 256 × 256,

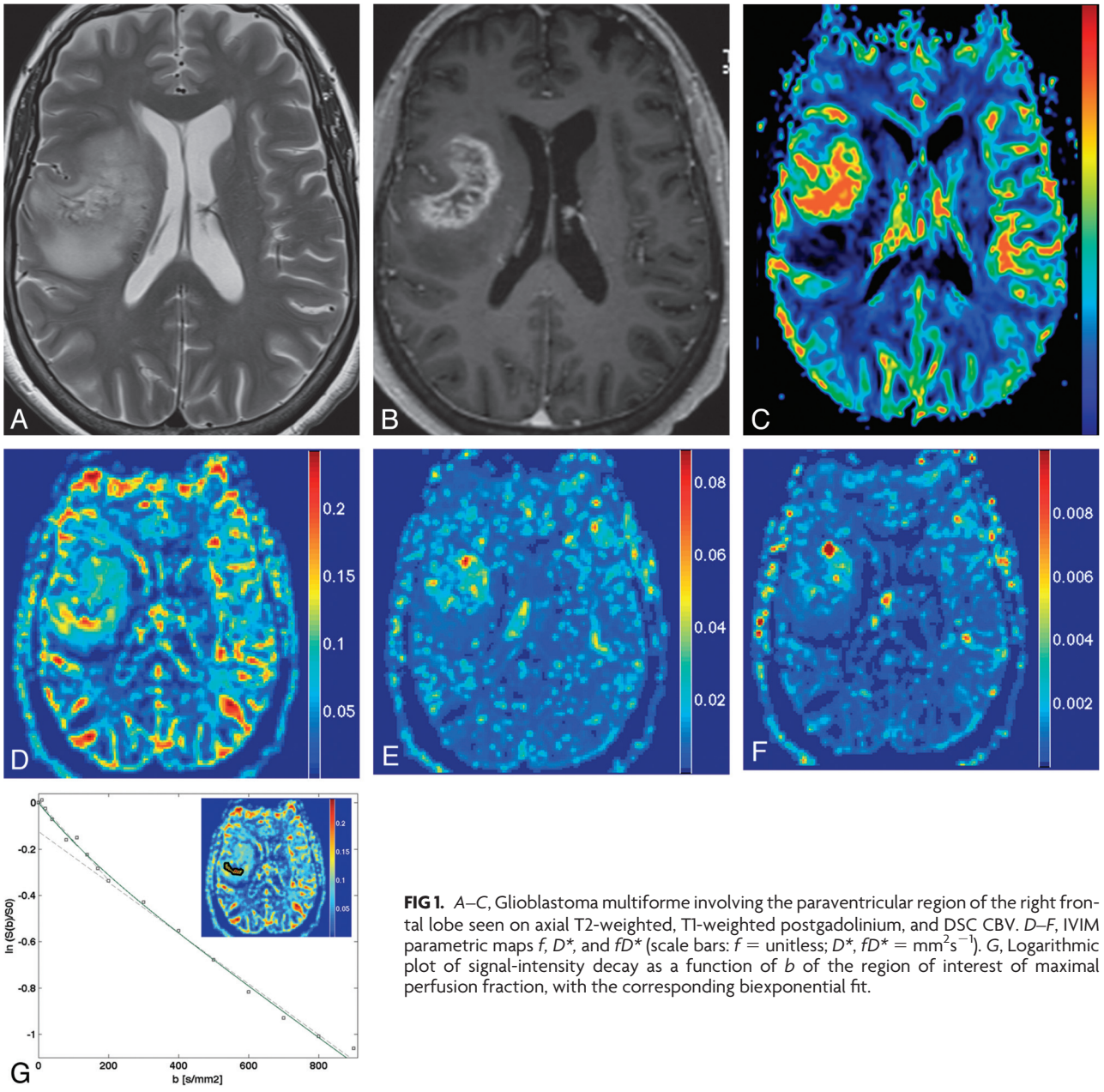

FIG 1. *A–C*, Glioblastoma multiforme involving the paraventricular region of the right frontal lobe seen on axial T2-weighted, T1-weighted postgadolinium, and DSC CBV. *D–F*, IVIM parametric maps *f*, *D**, and *fD** (scale bars: *f* = unitless; *D**, *fD** = mm^2s^{-1}). *G*, Logarithmic plot of signal-intensity decay as a function of *b* of the region of interest of maximal perfusion fraction, with the corresponding biexponential fit.

yielding an in-plane resolution of 1.2 × 1.2 mm^2. Parallel imaging, with an acceleration factor of 2 and a 75% partial Fourier encoding allowed TR/TE = 4000/99 ms. The receiver bandwidth was 1086 Hz/pixel, and fat was suppressed with a spectrally selective saturation routine. Total acquisition time was 3 minutes 7 seconds.

DSC MR Imaging

A gadolinium-based agent (gadoterate meglumine, Dotarem; Guerbet, Paris, France) was intravenously injected at a dose of 0.2 mL per kilogram of body weight and at a rate of 3 mL/s, followed by a 20-mL saline flush. Standard echo-planar images were consecutively acquired (TR = 1950 ms, TE = 43 ms, section thickness = 6 mm, FOV = 230 × 230, acquisition matrix = 128 × 128). No leakage correction was performed. CBV, MTT, and CBF maps were computed from the DSC MR imaging data by using the commercially available software, syngoMR (Siemens). On the section of interest, a region of interest was placed on an identified artery. We selected ≥4 voxels containing the best arterial input function curves, from which the average was built. We then set the time ranges defining baseline, gadolinium entry, and recovery, before the DSC perfusion maps were automatically calculated on the basis of a γ variate fitting of the time-concentration curve.

Regions of Interest

Brain gliomas have very heterogeneous structures and, accordingly, only the region with the highest malignancy defines the pathologic grade of the lesion. Therefore, a region of interest was manually placed on each tumor area in consensus by 2 experienced neuroradiologists (P.M. and P.H.) who were blinded to the histopathology, in the region of the tumor with maximal IVIM

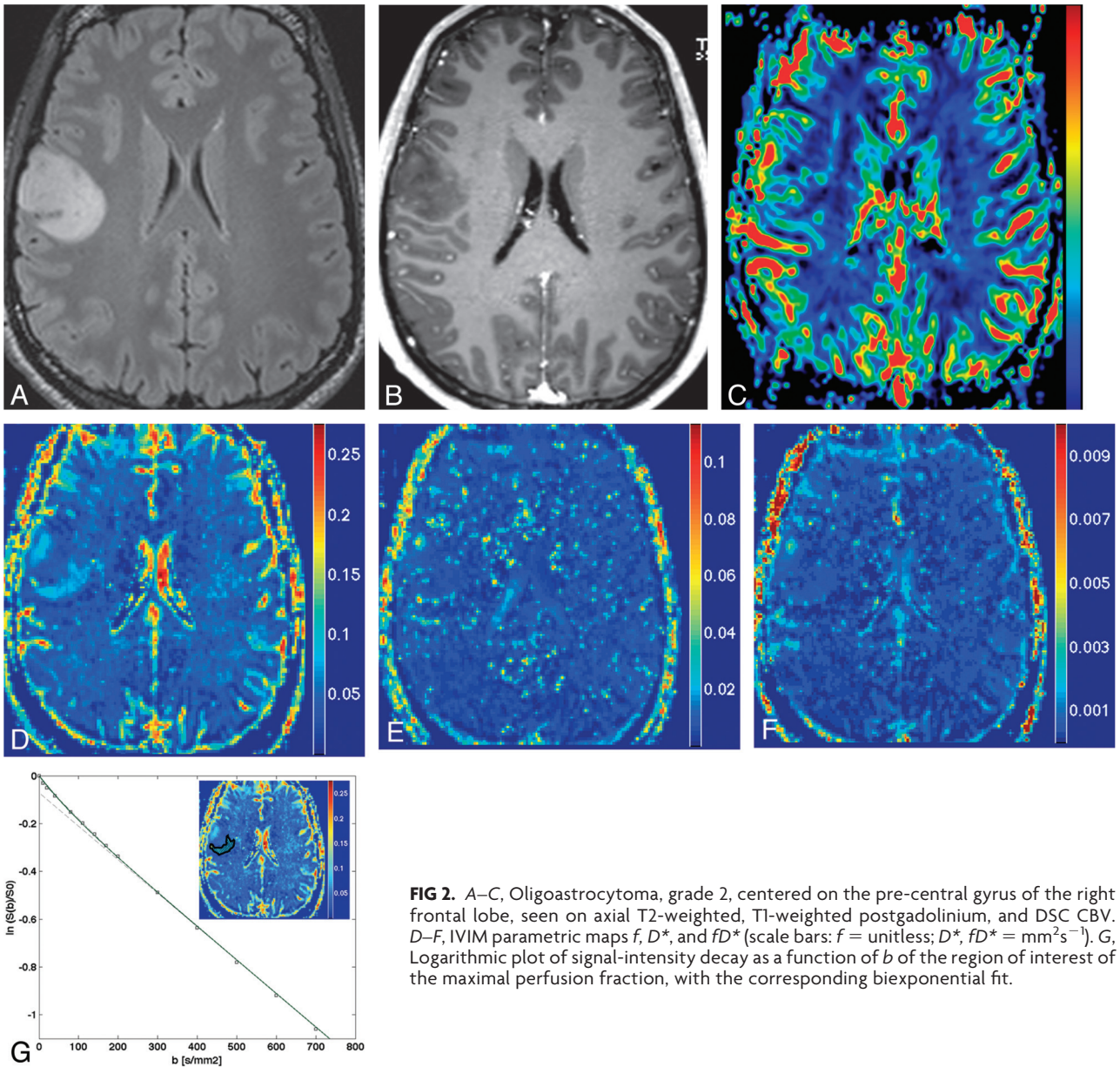

FIG 2. *A–C*, Oligoastrocytoma, grade 2, centered on the pre-central gyrus of the right frontal lobe, seen on axial T2-weighted, T1-weighted postgadolinium, and DSC CBV. *D–F*, IVIM parametric maps *f*, *D**, and *fD** (scale bars: *f* = unitless; *D**, *fD** = mm^2s^{-1}). *G*, Logarithmic plot of signal-intensity decay as a function of *b* of the region of interest of the maximal perfusion fraction, with the corresponding biexponential fit.

perfusion fraction and in the contralateral white matter, both on a single axial section. Cystic, hemorrhagic, or necrotic areas were avoided by using conventional pre- and postcontrast MR images. If a tumor was centered on the midline, a region of interest was chosen in the white matter of one of both hemispheres. Mean IVIM region-of-interest size was 322 ± 187 mm^2. The corresponding ROIs were then drawn on the DSC images, manually matching the images by using anatomic landmarks. The relative CBV was calculated by dividing the value of the region of interest in the tumor by the value of the contralateral normal-appearing white matter. The mean DSC region-of-interest size was 342 ± 151 mm^2.

We also produced histograms by placing a region of interest on all whole tumors on the IVIM b0 images, including all sections where the tumor was visible, and encompassing as much of the tumor area as possible but excluding cystic or necrotic areas, with the help of conventional pre- and postcontrast MR images. For the control histogram, a region of interest was placed in all patients to comprise the full white matter of an axial section of the contralateral hemisphere to the tumor.

All ROIs were placed so that they included as little CSF or as few large vessels as possible.

IVIM Image Processing

The standard IVIM 2-compartment diffusion model was assumed,[7] with a "microvascular" and a "nonvascular" compartment, having, respectively, a pseudodiffusion coefficient and an apparent diffusion coefficient. The percentage of incoherent signal arising from the microvascular compartment *f* is called the perfusion fraction. To obtain the IVIM parameters, the IVIM signal equation

$$\frac{S(b)}{S_0} = f \times e^{-bD^*} + (1-f) \times e^{-bD}$$

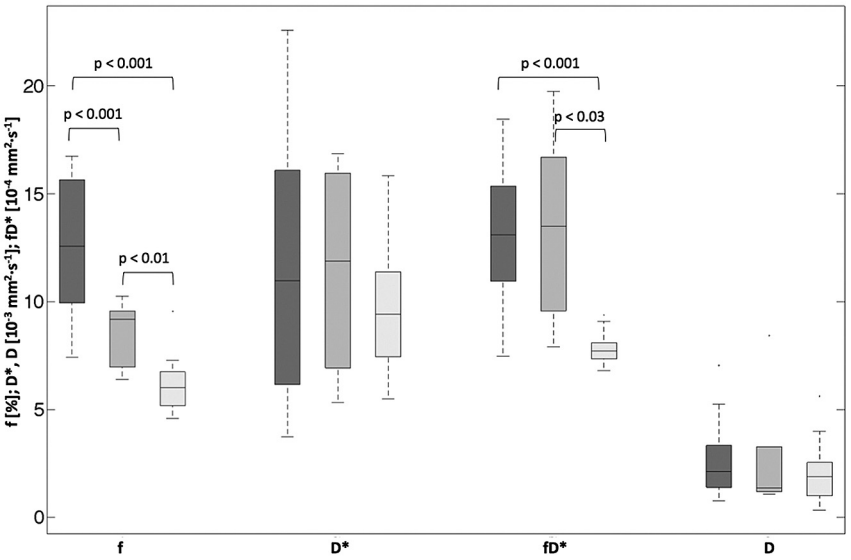

FIG 3. Box-and-whisker plot (median, 25th and 75th percentiles, minimum, maximum, and outliers) of *f, D*, fD*,* and *D,* as measured in ROIs of the maximum perfusion fraction. Dark gray indicates high-grade tumors; medium gray, low-grade tumors; light gray, contralateral control region of both high- and low- grade. *P* values are indicated when <.05.

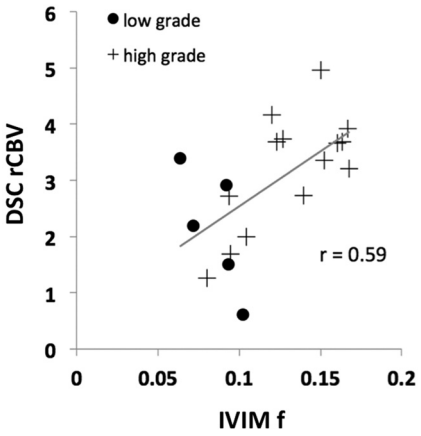

FIG 4. Scatterplots comparing relative DSC CBV (y-axis) with absolute IVIM *f* (x-axis). Pearson *r* correlation coefficient is given.

was fitted in 2 steps, as previously described,[20] first for $b > 200$ s/mm^2 for the single parameter D, then for all b and all parameters, while keeping D constant. This fit was done on a voxel-by-voxel basis, by using the Levenberg-Marquardt algorithm[21] implemented within Matlab (MathWorks, Natick, Massachusetts). This 2-step method increases robustness under biologic conditions and assumes that D^* is significantly greater than D[22] so that the influence of pseudodiffusion on signal decay can be neglected for b-values > 200 s/mm^2. Values under 0 for *f, D,* and D^*, and values with $f > 0.3$ and $D^* > 0.05$ mm^2/s were considered not physiologic and were set to 0.[23] This step excluded poorly fitted voxels (< 1% of the voxels) and was necessary to ensure that a single artifactually very high value in a single voxel could not be responsible for the measured effect, while also increasing the contrast of the IVIM maps.

Statistical Analysis

Statistical analysis was performed with Excel (Microsoft, Redmond, Washington). A normal distribution of the data was assumed. Single-tailed, pair-wise Student *t* tests were calculated when data were compared with the contralateral region. Single-tailed, 2-sample, unequal-variance Student *t* tests were calculated between high- and low-grade tumor groups. Statistical significance was defined at $P < .05$. The Pearson r correlation coefficient between IVIM perfusion fraction *f* and DSC CBV was calculated.

RESULTS

High-resolution IVIM perfusion maps were produced, and in tumorous regions, increased perfusion similar to DSC CBV could be observed (Figs 1 and 2).

In the region of interest of the maximum IVIM perfusion fraction, *f* was significantly higher in high-grade (0.127 ± 0.031) compared with low-grade gliomas (0.084 ± 0.016, $P = .0006$), as well as in both glioma groups compared with the contralateral region (0.061 ± 0.011, $P < .0001$) (Fig 3). Those results could be confirmed in the complementary study including the cohort of low-grade gliomas diagnosed on radiologic criteria only (On-line Fig 1).

f correlated moderately with DSC relative CBV ($r = 0.59$, Fig 4). The normalized histogram analysis of *f* over all whole tumor volumes showed an obvious "heavy-tailed" distribution for the high-grade gliomas in comparison with the low-grade and the reference contralateral white matter of an axial section (Fig 5).

No statistically significant difference was observed for D^* (0.0117 ± 0.0058 mm^{2}s^{-1} versus 0.0114 ± 0.0050 mm^{2}s^{-1} versus 0.0098 ± 0.0029 mm^{2}s^{-1}, for high-, low-grade, and contralateral brain, respectively; Fig 3). The flow-related parameter fD^* was not statistically significantly different between high- and low-grade tumors (0.00132 ± 0.00032 mm^{2}s^{-1} versus 0.00133 ± 0.00046 mm^{2}s^{-1}, respectively; $P = .46$), but it was significantly different between both glioma groups and the contralateral brain region (0.00077 ± 0.00007 mm^{2}s^{-1}, $P < .001$).

DISCUSSION

This report demonstrates that the IVIM perfusion fraction can help differentiate high- and low-grade gliomas. Of interest is the fact that this was obtained with a direct measurement in the tumor, without normalization with a measure in the contralateral white matter, as is currently done with DSC. While more data will be required for a detailed analysis, the following can be deduced from this small cohort: No low-grade tumor showed a value of *f* above 0.103, suggesting a probable high-grade histology when above this value, with a sensitivity of 75%. No control region showed an *f* value above 0.096, suggesting tumor when above this value, with a sensitivity of 69%.

Further, *f* correlated moderately with DSC CBV, confirming earlier results.[23] In the histogram analysis of all whole tumors, the heavy-tailed distribution for the high-grade in comparison with the low-grade gliomas and the reference white matter demon-

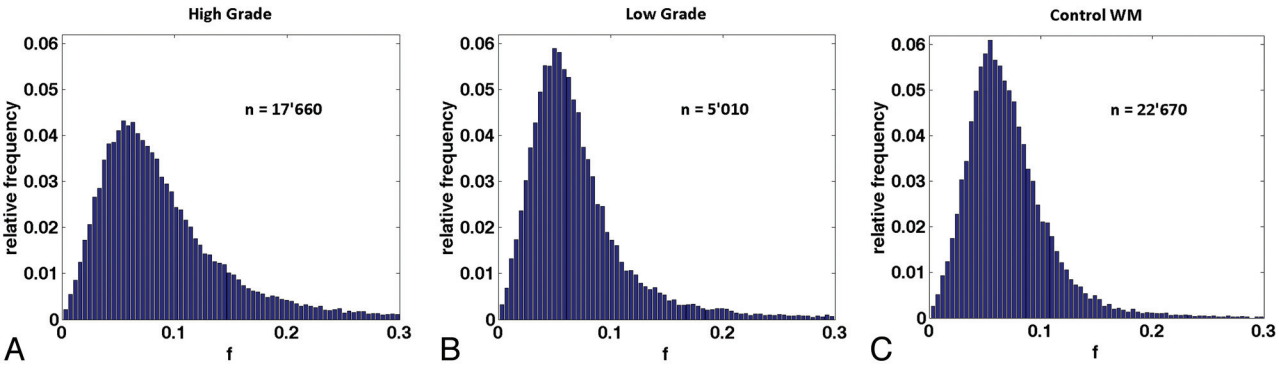

FIG 5. Normalized histograms of the perfusion fraction comprising the voxels of all whole tumor volumes for the high-grade (*A*) and low-grade (*B*) groups and for the control group (*C*). The total number of voxels included is indicated by *n*. An increase in the normalized number of highly perfused voxels can be observed in the high-grade tumor group in comparison with the low-grade and control groups.

strated that the presented effect can be measured independent of region-of-interest placement.

Single whole-tumor statistical analysis might be of interest but should be explored with care because tumor heterogeneity is a known property of gliomas and the region of highest malignancy defines the tumor grade.

There was no statistically significant difference between D^* in the different groups in this small cohort, which might be due to low signal-to-noise ratio. D^* has been shown to be less reproducible than f in the liver.[24] Nevertheless, in selected cases with high image quality (which was not an inclusion criterion for this study), we were able to produce D^* maps that were consistent with the known histologic diagnosis.[25] Furthermore, in a larger study with healthy volunteers over large regions of interest, a strong dependence of D^* (and no statistically significant dependence of f) on the cardiac cycle could be shown.[26] Together, these findings indicate that there is still hope that D^* could provide clinically relevant information when image quality is high enough.

There was also no statistically significant difference in D among the different groups. While regions with minimum apparent diffusion coefficient are thought to reflect the sites of highest cellularity within heterogeneous tumors and hence correlate with glioma grade,[27-29] those regions do not have to correspond necessarily to the regions of highest vascularity, which were studied here.

The known linear relationship[9] between the standard perfusion parameters and the IVIM perfusion parameters is dependent on the structure of the microvascular network, for example, on the mean vascular segment length or on the number and orientation of bifurcations. Neoangiogenic vessels in tumors are known to have a fundamentally different network structure than normal vessels.[30,31] This might, therefore, introduce a bias in the comparison with standard perfusion parameters, and further studies evaluating the exact relationship between IVIM and standard perfusion parameters in pathologic conditions should be pursued. The IVIM perfusion parameters should be considered as a new set of microperfusion parameters that, though related to the standard perfusion parameters, might differ in given cases, depending on the local microvascular network structure.

IVIM perfusion measurement in the brain remains technically challenging. It is obviously highly dependent on the immobility of the patient during the entire acquisition. Susceptibility inhomogeneities, such as around the petrous apex or the paranasal sinuses or due to the presence of metal or blood, for example, postoperatively, can harm the IVIM signal but are also problematic when performing DSC.

On the other hand, the IVIM method has many theoretic advantages over currently used DSC. It is intrinsically quantitative, and, because of the intravoxel excitation and readout, it does not require a precise knowledge of the arterial input function, which is challenging to measure.[32-34] It does not require contrast media and enables the acquisition of perfusion and diffusion information in a single sequence.

This study has several limitations. The cohort studied is relatively small, especially the low-grade tumors, because those tumors are usually followed without biopsy or operation at our institution. The results of a complementary study, including low-grade tumors as diagnosed on radiologic criteria only, can be found in the On-line Appendix and showed results similar to the ones presented. The placement of the ROIs was subjective in nature but reflected the usual clinical practice. Furthermore, the comparison between IVIM f and DSC CBV is limited by the fact that the DSC sections were positioned in the anterior/posterior commissure plane, while the IVIM sections were placed strictly transverse, but the regions of interest were sufficiently large to be identified reliably by using anatomic landmarks. In the future, the orientation and FOV of the different sequences could be aligned to ease comparison; however, this could be at the cost of optimal parameter settings, which are often sequence-specific. Coregistration and interpolation could improve the accuracy of the correspondence of the regions.

CONCLUSIONS

This report demonstrates that the IVIM perfusion fraction might be of value to differentiate high- and low-grade gliomas.

Disclosures: Christian Federau—*UNRELATED: Patents (planned, pending or issued)*: patent pending on IVIM.* Philippe Maeder—*UNRELATED: Patents (planned, pending or issued)*: patent pending on IVIM.* Patric Hagmann—*UNRELATED: patents (planned, pending or issued)*: patent pending on IVIM.* *Money paid to the institution.

REFERENCES

1. The Central Brain Tumor Registry of the United States. http://www.cbtrus.org. Accessed November 11, 2012
2. Surveillance, Epidemiology, and End Results (SEER) Program. National Cancer Institute. www.seer.cancer.gov. Accessed November 11, 2012

3. Aronen HJ, Gazit IE, Louis DN, et al. **Cerebral blood volume maps of gliomas: comparison with tumor grade and histologic findings.** *Radiology* 1994;191:41–51
4. Law M, Yang S, Wang H, et al. **Glioma grading: sensitivity, specificity, and predictive values of perfusion MR imaging and proton MR spectroscopic imaging compared with conventional MR imaging.** *AJNR Am J Neuroradiol* 2003;24:1989–98
5. Law M, Young RJ, Babb JS, et al. **Gliomas: predicting time to progression or survival with cerebral blood volume measurements at dynamic susceptibility-weighted contrast-enhanced perfusion MR imaging.** *Radiology* 2008;247:490–98
6. Kumar V, Abbas AK, Aster JC, et al. *Robbins & Cotran Pathologic Basis of Disease.* 7th ed. Paris, France: Elsevier Saunders; 2005
7. Le Bihan D, Breton E, Lallemand D, et al. **Separation of diffusion and perfusion in intravoxel incoherent motion MR imaging.** *Radiology* 1988;168:497–505
8. Stejskal EO, Tanner JE. **Spin diffusion measurements: spin echoes in the presence of a time-dependent field gradient.** *J Chem Phys* 1965;42:288–92
9. Le Bihan D, Turner R. **The capillary network: a link between IVIM and classical perfusion.** *Magn Reson Med* 1992;27:171–78
10. Sumi M, Van Cauteren M, Sumi T, et al. **Salivary gland tumors: use of intravoxel incoherent motion MR imaging for assessment of diffusion and perfusion for the differentiation of benign from malignant tumors.** *Radiology* 2012;263:770–77
11. Lemke A, Laun FB, Klauss M, et al. **Differentiation of pancreas carcinoma from healthy pancreatic tissue using multiple b-values: comparison of apparent diffusion coefficient and intravoxel incoherent motion derived parameters.** *Invest Radiol* 2009;44:769–75
12. Chandarana H, Kang SK, Wong S, et al. **Diffusion-weighted intravoxel incoherent motion imaging of renal tumors with histopathologic correlation.** *Invest Radiol* 2012;47:688–96
13. Sigmund EE, Cho GY, Kim S, et al. **Intravoxel incoherent motion imaging of tumor microenvironment in locally advanced breast cancer.** *Magn Reson Med* 2011;65:1437–47
14. Henkelman RM, Neil JJ, Xiang QS. **A quantitative interpretation of IVIM measurements of vascular perfusion in the rat brain.** *Magn Reson Med* 1994;32:464–69
15. Turner R, Le Bihan D, Maier J, et al. **Echo-planar imaging of intravoxel incoherent motion.** *Radiology* 1990;177:407–14
16. Neil JJ, Bosch CS, Ackerman JJ. **An evaluation of the sensitivity of the intravoxel incoherent motion (IVIM) method of blood flow measurement to changes in cerebral blood flow.** *Magn Reson Med* 1994;32:60–65
17. Chenevert TL, Pipe JG, Williams DM, et al. **Quantitative measurement of tissue perfusion and diffusion in vivo.** *Magn Reson Med* 1991;17:197–212
18. Le Bihan D, Moonen CT, van Zijl PC, et al. **Measuring random microscopic motion of water in tissues with MR imaging: a cat brain study.** *J Comput Assist Tomogr* 1991;15:19–25
19. Wirestam R, Brockstedt S, Lindgren A, et al. **The perfusion fraction in volunteers and in patients with ischaemic stroke.** *Acta Radiol* 1997;38:961–64
20. Federau C, Maeder P, O'Brien K, et al. **Quantitative measurement of brain perfusion with intravoxel incoherent motion MR imaging.** *Radiology* 2012;265:874–81
21. Seber GA, Wild CJ. *Nonlinear Regression.* Hoboken, New Jersey: Wiley-Interscience; 2003
22. Le Bihan D, Turner R, MacFall JR. **Effects of intravoxel incoherent motions (IVIM) in steady-state free precession (SSFP) imaging: applications to molecular diffusion imaging.** *Magn Reson Med* 1989;10:324–37
23. Wirestam R, Borg M, Brockstedt S, et al. **Perfusion-related parameters in intravoxel incoherent motion MR imaging compared with CBV and CBF measured by dynamic susceptibility-contrast MR technique.** *Acta Radiol* 2001;42:123–28
24. Andreou A, Koh DM, Collins DJ, et al. **Measurement reproducibility of perfusion fraction and pseudodiffusion coefficient derived by intravoxel incoherent motion diffusion-weighted MR imaging in normal liver and metastases.** *Eur Radiol* 2013;23:428–34
25. Federau C, O'Brien K, Meuli R, et al. **Measuring brain perfusion with intravoxel incoherent motion (IVIM): initial clinical experience.** *J Magn Reson Imaging* 2013. In press
26. Federau C, O'Brien K, Müller M, et al. **Pulsatile microvascular perfusion demonstrated in the human brain with intravoxel incoherent motion (IVIM) MRI.** In: *Proceedings of the 21st Annual Meeting of the International Society for Magnetic Resonance in Medicine*, Salt Lake City, Utah. April 20–26, 2013
27. Sugahara T, Korogi Y, Kochi M, et al. **Usefulness of diffusion-weighted MRI with echo-planar technique in the evaluation of cellularity in gliomas.** *J Magn Reson Imaging* 1999;9:53–60
28. Higano S, Yun X, Kumabe T, et al. **Malignant astrocytic tumors: clinical importance of apparent diffusion coefficient in prediction of grade and prognosis.** *Radiology* 2006;241:839–46
29. Murakami R, Sugahara T, Nakamura H, et al. **Malignant supratentorial astrocytoma treated with postoperative radiation therapy: prognostic value of pretreatment quantitative diffusion-weighted MR imaging.** *Radiology* 2007;243:493–99
30. Scatliff JH, Radcliffe WB, Pittman HH, et al. **Vascular structure of glioblastomas.** *Am J Roentgenol Radium Ther Nuclear Med* 1969;105:795–805
31. Jain RK, di Tomaso E, Duda DG, et al. **Angiogenesis in brain tumours.** *Nat Rev Neurosci* 2007;8:610–22
32. Calamante F, Gadian DG, Connelly A. **Quantification of perfusion using bolus tracking magnetic resonance imaging in stroke: assumptions, limitations, and potential implications for clinical use.** *Stroke* 2002;33:1146–51
33. Knutsson L, Stahlberg F, Wirestam R. **Absolute quantification of perfusion using dynamic susceptibility contrast MRI: pitfalls and possibilities.** *MAGMA* 2010;23:1–21
34. Petersen ET, Zimine I, Ho YC, et al. **Non-invasive measurement of perfusion: a critical review of arterial spin labelling techniques.** *Br J Radiol* 2006;79:688–701